



HAL
open science

Modelling the growth stress distribution in tree branches: impact of different growth strategies

A van Rooij, Eric Badel, Jean-François Barczi, Yves Caraglio, Tancrede Almeras, Joseph Gril

► To cite this version:

A van Rooij, Eric Badel, Jean-François Barczi, Yves Caraglio, Tancrede Almeras, et al.. Modelling the growth stress distribution in tree branches: impact of different growth strategies. 2022. hal-03748026v2

HAL Id: hal-03748026

<https://hal.science/hal-03748026v2>

Preprint submitted on 25 Aug 2022 (v2), last revised 21 Nov 2023 (v6)

HAL is a multi-disciplinary open access archive for the deposit and dissemination of scientific research documents, whether they are published or not. The documents may come from teaching and research institutions in France or abroad, or from public or private research centers.

L'archive ouverte pluridisciplinaire **HAL**, est destinée au dépôt et à la diffusion de documents scientifiques de niveau recherche, publiés ou non, émanant des établissements d'enseignement et de recherche français ou étrangers, des laboratoires publics ou privés.

1 Modelling the growth stress in tree branches: impact of different growth
2 strategies

3 A. Van Rooij^{1,2}, E. Badel², J.F. Barczi³, Y. Caraglio³, T. Alméras⁴ and J. Gril^{1,2}

- 4 1. Université Clermont-Auvergne, CNRS, Institut Pascal, F-63000, Clermont-Ferrand, France
5 2. Université Clermont-Auvergne, INRAE, PIAF, F-63000, Clermont-Ferrand, France
6 3. CIRAD, Unité Mixte de Recherche (UMR) Cirad-Cnrs-Inra-Ird-Université Montpellier 2, 'botAnique
7 et bioinforMatique de l'Architecture des Plantes' (AMAP), A-51/PS2, Boulevard de la Lironde, 34398
8 Montpellier cedex 5, France
9 4. LMGC, CNRS, Université of Montpellier, Montpellier, France

10 **Abstract**

11 This work aims to model the mechanical consequences of different strategies used by tree branches to
12 ensure their posture despite the increasing loading due to gravity. The two known strategies of a branch to
13 straighten itself are the asymmetry of maturation stress, including reaction wood formation, and eccentric
14 growth. Both strategies can be observed in nature and influence the stress distribution developed in the
15 branch each year. This so-called growth stress reflects the mechanical state of the branch. In this work,
16 a growth stress model was developed at the cross-section level in order to quantify the bio-mechanical
17 impact of each strategy. For illustration, this model was applied to the branches of two 50-year-old trees,
18 one softwood *Pinus pinaster* and one hardwood *Prunus avium*, both simulated with the AMAPSim finite
19 element software. The model show that in hardwoods, both strategies are efficient and that the combination
20 of the two is optimal. In softwoods, the model shows that eccentricity process is less efficient. Moreover,
21 eccentricity process does not necessarily act as a relevant lever for postural control. However eccentricity
22 process greatly modify the profile pattern of mechanic stress. This work opens exciting experimental
23 perspectives in order to understand the biomechanical process involved in the building of branches.

24 Abbreviations and notations (in order of occurrence)

NW, TW, CW	Normal Wood, Tension Wood, Compression Wood
(x, y, z)	Local reference system associated with the section
O	Centre of the section
r, R	Radii of the cross section (m)
$e(R), \bar{e}(R)$	Eccentricity at the stem radius R, integrated eccentricity up to $r = R$
(x', y', z')	Local reference system associated with the section, centred on the pith
σ	Stress (MPa)
σ_0	Induced maturation stress (Mpa)
S	Cross section area (m^2)
N, M	Loads (N): normal force parallel to z' and bending moment around y'
E	Module of elasticity in L direction (GPa): MOE
μ	Induced maturation strain
ϵ, a, b	Deformations: strain at the center, changes in curvature around x, y
K_i	Structural stiffness of the cross-section
F_i	External coefficients (maturation and load)
θ	Circumferential position in section (rad)
$\sigma_0(\theta)$	Maturation strain in the new ring at circumferential position θ
α	Mean maturation stress in the new ring
β	Differential stress in the new ring
$r_{x'y'}$	Radius of the cross section at the instant of appearance of the point (x', y')
$\lambda_N, \lambda_M, \nu_M, \nu_N$	Load power law: allometric coefficient
λ_b, ν_b	Change of curvature power law: allometric coefficient
$\sigma_{NW}, \sigma_{TW}, \sigma_{CW}$	Maturation stress in the normal wood, tension wood and compression wood
\vec{N}_n, \vec{M}_n	Loads of growth unit n: normal force and bending moment around y
N_z, M_x, M_y, M_z	Loads of growth unit n: projection of \vec{N}_n on \vec{z} and bending moment \vec{M}_n around $\vec{x}, \vec{y}, \vec{z}$
m_n	Mass of the growth unit n (kg)
g	Acceleration of gravity: $g = 9.8 \text{ m.s}^{-2}$
G_n	Centre of gravity of the growth unit n
E_d, E_g	Green, air-dry MOE
ρ	Density
$\mu_{NW}, \mu_{TW}, \mu_{CW}$	Maturation strain in the normal wood, tension wood and compression wood
μ_{strain}	$1/10^6$
D_n, D_{n+1}	First and second diameter the growth unit n
D	Deflection of a growth unit
L_n	Length of the growth unit n

27 Introduction

28 From a mechanical point of view, wood in tree fulfils three major functions: construction of the architecture,
 29 postural maintenance and resistance to external elements [Thibaut (2019)]. These three functions are
 30 provided by the way wood cells differentiate and accumulate. Each axis of a tree can be considered as an
 31 inclined beam, consisting of a succession of conical growth units [Barthélémy and Caraglio (2007)]. It
 32 is built in two steps: primary growth resulting in new growth units that increase the length of the axis;
 33 secondary growth resulting in thickening of already existing units by addition of annual rings. These two
 34 interactive and additional processes lead to a specific pattern of mechanical stress, called 'growth stress',
 35 superposition of support stress and maturation stress [Archer (1976); Fournier et al. (1991a)]. The support
 36 stress results from the continuous increase of the weight supported by the axis over the years. It vanishes

37 near stem periphery where the recently formed wood contributes to the support of recently produced
38 biomass only, and reaches maximal levels in the core of the stem. Maturation stress is set up at the end of
39 the cell-wall maturation process, when molecular components such as lignin polymerise, generating growth
40 forces by small dilatation or contraction restrained by the rigidity of the previously formed wood cells
41 [Alméras and Clair (2016)]. An evaluation of the maturation stress can be obtained by measuring the
42 strain associated to stress release at stem periphery, where no support stress is present [Nicholson (1971);
43 Yoshida and Okuyama: (2002); Yang et al. (2005)]. The circumferential heterogeneity of this peripheral
44 stress is needed to regulate stem curvature. In most cases, a tensile maturation stress is produced in the
45 newly formed 'normal wood' (NW). But observations on inclined trunks [Alméras et al. (2005); Coutand
46 et al. (2007); Thibaut and Gril (2021)], seedlings [Hung et al. (2016)] and branches [Fisher and Stevenson
47 (1981); Huang et al. (2010); Tsai et al. (2012); Hung et al. (2017)] have evidenced a clear difference
48 between hardwoods and softwoods trees. Hardwoods are able to produce 'tension wood' (TW) inducing a
49 much higher tensile stress on one side, while for softwood a compressive stress is induced in 'compression
50 wood' (CW). The first pulls, the second pushes. In the most usual case of an inclined stem restoring
51 vertical orientation, TW is formed on the upper side and CW on the lower; but other situations can be
52 encountered depending on the biomechanical requirements of the tree [Wang et al. (2009)]. In addition to
53 their participation in the postural control of tree stems, these two types of so-called 'reaction wood' (RW)
54 are characterised by a different anatomy (not discussed here) and specific physical and mechanical properties.

55
56 Growth stress modelling plays an important role in the understanding of the phenomena involved in
57 the orientation process of a stem. The history of biomechanical models begins with Kübler (1959) who
58 proposed an analytical formulation of growth stress for a perfect cylinder made of a homogeneous and
59 transversally isotropic wood. Later, Archer and Byrnes (1974) took into account an asymmetry of the
60 maturation stresses, and Fournier et al. (1991a,b) proposed a semi-incremental version of these models,
61 allowing to take into account a potential gradient of mechanical parameters (stiffness, maturation). By
62 associating their previous model to the loading induced by the tree weight, Fournier et al. (1994) made
63 the connection between growth stress and stem orientation. To understand the parameters involved in
64 orientation of the stems, this model has been taken up and developed by several authors. Yamamoto
65 et al. (2002) added a primary shoot and went back to curvature calculations. Alméras and Fournier (2009)
66 introduced the notion of gravitropic performance (capacity of the tree to correct the bending moment
67 induced by its weight) and gave criteria of long-term stability. Huang et al. (2005) and Alméras et al.
68 (2005) also made the model more realistic by introducing the pith eccentricity and by introducing spatial
69 heterogeneity of stiffness, which allowed them to quantify the effectiveness of eccentricity, maturation,
70 stiffness gradient and initial radius in the curvature correction process. They both showed that the main
71 factor in the gravitropic correction process is the distribution of the maturation stresses. Still in line
72 with Fournier's 1994 model, Alméras et al. (2018) recently developed analytical models of longitudinal
73 growth stresses, taking into account different configurations, like eccentricity or maturation gradient, and
74 evolution laws, like evolution of stiffness per additional layer. Finally, based on the same philosophy as
75 that established by Kübler, tree-scale and finite-element models have emerged [Fourcaud et al. (2003);
76 Ancelin et al. (2004)].

77
78 Most of these models have been applied to trunks. Some theoretical predictions have been made on inclined
79 trunks [Alméras and Fournier (2009)] and only one analytical work has been done so far on branches
80 [Huang et al. (2010)]. Branches are particular axes subject to large inclinations, and some assumptions
81 such as uniformity of eccentricity find their limits. The only model proposing an integration of the stress
82 on the whole section, proposed by Fourcaud et al. (2003), did not take into account the eccentricity at all.
83 Huang et al. (2005) and Alméras et al. (2005) have quantified the roles of maturation and eccentricity in
84 the recovery process, but have not evaluated their ability to ensure an imposed growth scenario.
85 In this framework, we propose a semi-incremental biomechanical model of growth stress at the cross section

86 level that takes into account the eccentricity and maturation gradients during the building of branches.
 87 Using the digital models of a hardwood and a softwood, the impact of each of these two straightening
 88 strategies on the stress state will be evaluated.

89 Material and methods

90 Numerical model

91 General hypotheses

92 The problem will be set in the framework of beam theory. From a geometrical point of view, branches
 93 generally show profiles that are well suited to this type of analytical framework: slender shape, no important
 94 diameter variations. The shape effects due to twigs and other local biological phenomena (cavity, nodes,
 95 etc.) are neglected. The same set of hypotheses as in Alm eras et al. (2018) is adopted. In this study,
 96 we focus on the behaviour in the longitudinal direction (parallel to the main axis). Horizontal bending
 97 and torsion loads are not considered. Only the vertical bending moment (that caused by the weight) is
 98 considered. These initial hypotheses on the loading modes will be discussed later.

99 Geometrical settings

100 The object of study is the cross-section of a branch, placed within a plane locally orthogonal to the pith.
 101 The local reference frame of the section is $(\vec{x}, \vec{y}, \vec{z})$, with \vec{z} the longitudinal direction of the axis, and \vec{x}
 102 placed in a vertical plane and facing upwards (Figure 1). The shape of the cross-section is assumed to
 103 be circular at any stage of development, described by the successive deposition of wood rings. The term
 104 of 'ring' refers here to the volume occupied by wood cells produced by the cambium during a certain
 105 duration of time, not necessarily annual: it must be taken in a numerical sense. These rings possibly
 106 present an eccentricity resulting from asymmetry of secondary growth. Since the model only takes into
 107 account vertical bending, the eccentricity is set along the x axis, as expressed by the following equation:

$$O(t) = \int_0^{R(t)} e(r) dr = \bar{e}R(t) \quad (1)$$

108 with $O(t)$ the position of the geometrical centre and $R(t)$ the radius of the section at time t , $e(r)$ the
 109 eccentricity when the stem radius was r and \bar{e} the integrated eccentricity up to $r = R$. The eccentricity
 110 varies in the interval $[-1, 1]$. A zero eccentricity corresponds to a centred section, while -1 or 1 corresponds
 111 to maximum eccentricity resulting from secondary growth only on the lower or the upper side of the
 112 section, respectively. In the following, the position x' in the pith reference frame will be needed. By calling
 113 x the vertical position in the geometrical reference frame, we deduce from equation 1:

$$x = x' - \bar{e}R \quad (2)$$

114 Computation of the mechanical behaviour

115 We will develop a radial incremental method. For each radial increment, the longitudinal stress is computed
 116 so as to satisfy the static equilibrium of the cross section:

$$\left\{ \begin{array}{l} \int_S \delta\sigma dS + \int_{\delta S} \sigma_0 dS = \delta N \\ \int_S \delta\sigma x dS + \int_{\delta S} \sigma_0 x dS = -\delta M \end{array} \right. \quad (3a)$$

$$\left\{ \begin{array}{l} \int_S \delta\sigma dS + \int_{\delta S} \sigma_0 dS = \delta N \\ \int_S \delta\sigma x dS + \int_{\delta S} \sigma_0 x dS = -\delta M \end{array} \right. \quad (3b)$$

117 where S is the cross-section and δS its increment, $\delta\sigma$ the increment of stress σ in the already formed wood,
 118 in response to the maturation stress σ_0 generated in the new wood layer, δN and δM the increment of

119 external force N and bending moment M , respectively, applied on the cross-section. For illustration, the
 120 geometric situation for K rings and an increment of stem radius δR is proposed in Figure 1.

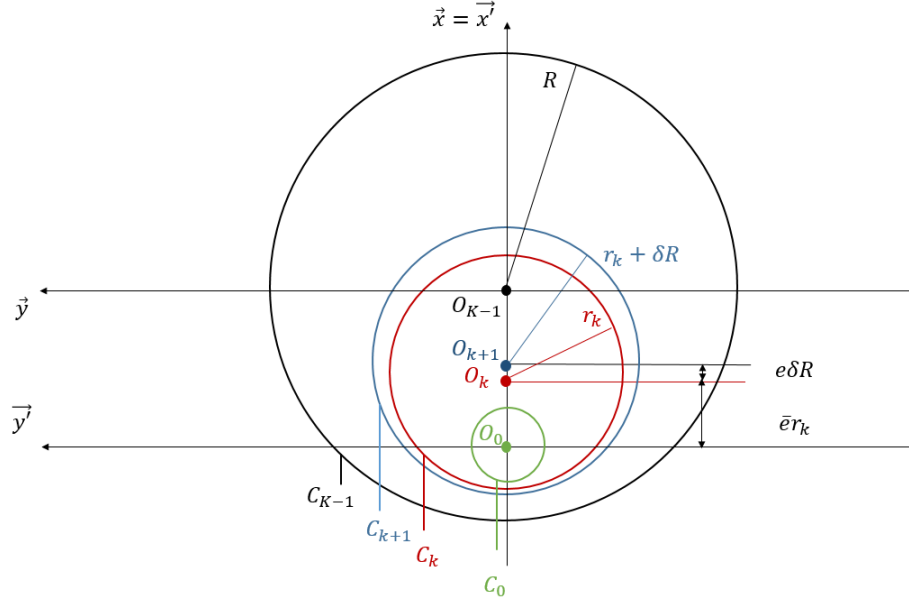


Figure 1: Geometrical representation of a section with K numerical rings and a radial increment δR between rings $k - 1$ and k .

121

122 The stress σ is linked to the strain ϵ by a pre-stressed Hooke law:

$$\sigma = E(\epsilon - \mu) = E\epsilon + \sigma_0 \quad (4)$$

123 with E the longitudinal Young's modulus, μ the maturation strain and σ_0 the maturation stress. In the
 124 context of the beam theory, the planar sections remain planar sections (Euler-Bernouilli assumption), so
 125 that the strain field is described by the deformation a at the centre of the pith and the curvature b relative
 126 to the y -axis:

$$\delta\epsilon = \delta a + x\delta b \quad (5)$$

127 where $\delta\epsilon$, δa , δb are the increments of ϵ , a , b , respectively. The stress increment $\delta\sigma$, in the already formed
 128 wood where no maturation occurs anymore, can then be deduced:

$$\delta\sigma = E\delta\epsilon = E(\delta a + x\delta b) \quad (6)$$

From these considerations, the system (3) becomes (details of the calculation are given in Appendix A):

$$\begin{cases} K_0\delta a + K_1\delta b = \delta F_0 \\ K_1\delta a + K_2\delta b = \delta F_1 \end{cases} \quad (7a)$$

$$\quad (7b)$$

129 with

$$K_0 = E\pi R^2, \quad K_1 = E\pi\bar{e}R^3, \quad K_2 = E\pi R^4 \left(\bar{e}^2 + \frac{1}{4} \right) \quad (8)$$

$$\delta F_0 = - \int_{\delta S} \sigma_0 dS + \delta N, \quad \delta F_1 = - \int_{\delta S} \sigma_0 x dS - \delta M$$

130 The calculation of the coefficients δF_0 and δF_1 depends on the formulation of the maturation stress. The
 131 maturation stress is assumed to vary circumferentially as follows:

$$\sigma_0(\theta) = \alpha + \beta \cos \theta \quad (9)$$

where the mean stress α and differential stress β are defined differently in softwood and hardwood species:

$$\left\{ \begin{array}{l} \text{Hardwood: } \alpha = \frac{\sigma_{TW} + \sigma_{NW}}{2}; \beta = \frac{\sigma_{TW} - \sigma_{NW}}{2} \\ \text{Softwood: } \alpha = \frac{\sigma_{CW} + \sigma_{NW}}{2}; \beta = \frac{\sigma_{NW} - \sigma_{CW}}{2} \end{array} \right. \quad (10a)$$

$$\left\{ \begin{array}{l} \text{Hardwood: } \alpha = \frac{\sigma_{TW} + \sigma_{NW}}{2}; \beta = \frac{\sigma_{TW} - \sigma_{NW}}{2} \\ \text{Softwood: } \alpha = \frac{\sigma_{CW} + \sigma_{NW}}{2}; \beta = \frac{\sigma_{NW} - \sigma_{CW}}{2} \end{array} \right. \quad (10b)$$

with σ_{TW} (resp. σ_{CW}) the maturation stress in the tension wood (resp. compression wood), and σ_{NW} the stress in the opposite wood (normal wood). One gets :

$$\left\{ \begin{array}{l} \delta F_0 = -\pi R (2\alpha + e\beta) \delta R + \delta N \\ \delta F_1 = -\pi R^2 (3\alpha e + e^2\beta + \beta) \delta R - \delta M \end{array} \right. \quad (11a)$$

$$\left\{ \begin{array}{l} \delta F_0 = -\pi R (2\alpha + e\beta) \delta R + \delta N \\ \delta F_1 = -\pi R^2 (3\alpha e + e^2\beta + \beta) \delta R - \delta M \end{array} \right. \quad (11b)$$

132 From equations (8), (11a) and (11b), the components of the system (7) are known. By inversion, $\delta\alpha$ and
133 δb can be obtained:

$$\left\{ \begin{array}{l} \delta a = \frac{4}{ER} \left[\left(3e\bar{e} - 2e^2 - \frac{1}{2} \right) \alpha - \left(\bar{e} - \frac{e}{4} \right) \beta \right] \delta R - \frac{4}{E\pi R^3} \left[\bar{e}\delta M + \left(\bar{e} + \frac{1}{4} \right) R\delta N \right] \\ \delta b = \frac{4}{ER^2} \left[- (3e - 2\bar{e}) \alpha - \left(e^2 - e\bar{e} + 1 \right) \beta \right] \delta R - \frac{4}{E\pi R^4} (\delta M + \bar{e}R\delta N) \end{array} \right. \quad (12a)$$

$$\left\{ \begin{array}{l} \delta a = \frac{4}{ER} \left[\left(3e\bar{e} - 2e^2 - \frac{1}{2} \right) \alpha - \left(\bar{e} - \frac{e}{4} \right) \beta \right] \delta R - \frac{4}{E\pi R^3} \left[\bar{e}\delta M + \left(\bar{e} + \frac{1}{4} \right) R\delta N \right] \\ \delta b = \frac{4}{ER^2} \left[- (3e - 2\bar{e}) \alpha - \left(e^2 - e\bar{e} + 1 \right) \beta \right] \delta R - \frac{4}{E\pi R^4} (\delta M + \bar{e}R\delta N) \end{array} \right. \quad (12b)$$

134 Once δa and δb are known, the stress increment $\delta\sigma$ at any position given by (x', y') can be obtained from
135 (6). The stress distribution at this position can be obtained as the sum of the initial maturation stress and
136 all the stress increments undergone by the material point since its creation.

$$\sigma(x', y', R) = \sigma_0(x', y') + \sum_{k=k_{x'y'}}^K \delta\sigma_k \quad (13)$$

137 where $\delta R_k = r_k - r_{k-1}$ for a succession of ring radii $r_0 = 0 < r_0 < \dots < r_k < \dots < r_K = R$, $\delta\sigma_k$ is the
138 corresponding increment, and $k_{x'y'}$ designates the ring containing the point.

139 Analytical formulations

140 When each incremental term in expression (12b) is divided by dR and dR tends to zero, the ratio tends to
141 the derivative against R , leading to (see details in Appendix B):

$$\left\{ \begin{array}{l} \frac{da}{dR} = \frac{4}{ER} \left[\left(3e\bar{e} - 2e^2 - \frac{1}{2} \right) \alpha - \left(\bar{e} - \frac{e}{4} \right) \beta - \frac{1}{\pi R^2} \left(\bar{e} \frac{dM}{dR} + \left(\bar{e} + \frac{1}{4} \right) R \frac{dN}{dR} \right) \right] \\ \frac{db}{dR} = \frac{4}{ER^2} \left[- (3e - 2\bar{e}) \alpha - \left(e^2 - e\bar{e} + 1 \right) \beta - \frac{1}{\pi R^2} \left(\frac{dM}{dR} + \bar{e}R \frac{dN}{dR} \right) \right] \end{array} \right. \quad (14a)$$

$$\left\{ \begin{array}{l} \frac{da}{dR} = \frac{4}{ER} \left[\left(3e\bar{e} - 2e^2 - \frac{1}{2} \right) \alpha - \left(\bar{e} - \frac{e}{4} \right) \beta - \frac{1}{\pi R^2} \left(\bar{e} \frac{dM}{dR} + \left(\bar{e} + \frac{1}{4} \right) R \frac{dN}{dR} \right) \right] \\ \frac{db}{dR} = \frac{4}{ER^2} \left[- (3e - 2\bar{e}) \alpha - \left(e^2 - e\bar{e} + 1 \right) \beta - \frac{1}{\pi R^2} \left(\frac{dM}{dR} + \bar{e}R \frac{dN}{dR} \right) \right] \end{array} \right. \quad (14b)$$

142 If the division by δR is applied to the stress σ , a function of the stem radius R and the position x' , the
143 partial derivative $\partial\sigma/\partial R$ is obtained, so that equation (13) becomes:

$$\sigma(x', y', R) = \sigma_0(x', y') + \int_{r_{x'y'}}^R \frac{\partial\sigma}{\partial R}(x', R') dR' \quad (15)$$

144 by calling $r_{x'y'}$ the radius of the section at the instant of appearance of the point with coordinates (x', y') .

The expressions of axial force $N(R)$ and bending moment $M(R)$ are needed to compute the evolution of the stress distribution in the cross section. For this purpose, we assume that they vary as a power function of the radius. This results in the following allometric laws:

$$\begin{cases} N = \lambda_N R^{\nu_N} \\ M = \lambda_M R^{\nu_M} \end{cases} \quad \begin{matrix} (16a) \\ (16b) \end{matrix}$$

with $\lambda_{N,M}$ and $\nu_{N,M}$ allometric coefficients. The λ -coefficients are directly proportional to the weight supported by the cross section, either that of the branch itself or that of axes of higher orders. The ν -coefficients express the kinetics of the secondary growth: a small ν refers to an early secondary growth, a higher one to a later diameter increase.

The calculation of σ requires also the knowledge of the curvature rate $\frac{db}{dr}$. In most of the cases we will assume the stationarity of the branch orientation. This results in $\frac{db}{dr} = 0$ and the fact that the branch balances its weight increment at every deposition of a new wood layer. However, we can consider two cases for which the branch does not build up in a stationary way: passive bending (under its own weight), and up-righting (the action of maturation is stronger than the additional weight). In both cases, the change in curvature has been calculated by Alm eras and Fournier (2009) and Alm eras et al. (2018) as follows:

$$\begin{cases} \text{Up-righting:} & \frac{db}{dr} = -4 \frac{\beta}{Er^2} \\ \text{Passive bending:} & \frac{db}{dr} = 4 \frac{\lambda_M \nu_M}{E\pi} r^{\nu_M-5} \end{cases} \quad \begin{matrix} (17a) \\ (17b) \end{matrix}$$

For the calculation, we will then take a general law:

$$\frac{db}{dr} = \lambda_b r^{\nu_b} \quad (18)$$

Combining (14),(15),(16) and (18), the total stress can then be computed as (detail in Appendix C):

$$\sigma^i(x', y', R) = \sigma_0^i(x', y') + S_1 \ln \left(\frac{R}{r_{x'y'}} \right) + \frac{S_2}{S_3} \left(R^{S_2} - r_{x'y'}^{S_2} \right) + \frac{S_4}{S_5} \left(R^{S_5} - r_{x'y'}^{S_5} \right) + \frac{S_6}{S_7} \left(R^{S_7} - r_{x'y'}^{S_7} \right) x' \quad (19)$$

where $S_1 = -2\alpha + \beta e$ is driven by the maturation process, $S_2 = \frac{\lambda_N \nu_N}{\pi}$ and $S_3 = \nu_N - 2$ by branch loading (geometric evolution of the branch), $S_4 = -E\bar{e}\lambda_b$ and $S_5 = \nu_b + 2$ by the orientation of the branch when eccentricity occurs, $S_6 = E\lambda_b$ and $S_7 = \nu_b + 1$ by the orientation of the branch.

For each radius r , the remaining unknowns are the mean stress α , the differential stress β and the eccentricity e . Equation (14b) can be rewritten as:

$$(3e - 2\bar{e})\alpha + (e^2 - e\bar{e} + 1)\beta = \frac{-1}{\pi r^2} \left(\frac{dM}{dR} + \bar{e}R \frac{dN}{dR} \right) - E \frac{R^2}{4} \frac{db}{dR} \quad (20)$$

Thus by fixing two parameters, the third is directly determined. The maturation parameters α and β being determined by the maturation stress in normal wood σ_{NW} and reaction wood σ_{TW} or σ_{CW} according to (10), these parameters will be managed.

We will consider two possible configurations for the simulations in next section:

-
1. First, we apply a constant eccentricity (so that $\bar{e} = e$) and we fix the stress level in the normal wood. In that case, the maturation stress of the reaction wood is given by equations (10):

$$\left\{ \begin{array}{l} \sigma_{TW} = \frac{-2}{\pi r^2(1+e)} \left(\frac{dM}{dr} + er \frac{dN}{dr} \right) + \sigma_{NW} \left(\frac{1-e}{1+e} \right) + \lambda_b \left(\frac{Er^2}{2(1+e)} \right) r^{\nu_b} \\ \sigma_{CW} = \frac{2}{\pi r^2(1-e)} \left(\frac{dM}{dr} + eR \frac{dN}{dr} \right) + \sigma_{NW} \left(\frac{1+e}{1-e} \right) - \lambda_b \left(\frac{Er^2}{2(1-e)} \right) r^{\nu_b} \end{array} \right. \quad (21a)$$

$$\left\{ \begin{array}{l} \sigma_{CW} = \frac{2}{\pi r^2(1-e)} \left(\frac{dM}{dr} + eR \frac{dN}{dr} \right) + \sigma_{NW} \left(\frac{1+e}{1-e} \right) - \lambda_b \left(\frac{Er^2}{2(1-e)} \right) r^{\nu_b} \end{array} \right. \quad (21b)$$

- 161 2. Second, we fix the maturation parameters and we observe how the branch straighten, or not, just by
 162 varying the eccentricity of the secondary growth. In this configuration, equation 14b becomes a two
 163 degree equation in e that can be solved numerically.

164 In these two configurations, using data on the support allometries $\lambda_N, \lambda_M, \nu_M, \nu_N$ we can calculate the
 165 stress in the reaction wood and/or the eccentricity with different (λ_b, ν_b) , then deduce the growth stress
 166 profile in the section (eq. 19). In the next part, we will see how the allometric coefficients can be obtained
 167 from realistic growth data.

168 Realistic growth data

169 Tree material

170 Numerical experiments were carried out using two reference models: one softwood *Pinus Pinaster* and
 171 one hardwood *Prunus avium* (Fig 2). Both their architectures follow Rauh's model, meaning that the
 172 branching is rhythmic, the axes monopodial and the branches orthotropic [Hallé et al. (1978)]. The digital
 173 trees were computed with AMAPSim software [Barczi et al. (2007)]. Architectural parameters were
 174 obtained by observations and field studies: Coudurier et al. (1993) and Heuret et al. (2006) for *Pinus*
 175 *pinaster*, Caraglio (1996) and Barthélémy et al. (2009) for *Prunus avium*.



Figure 2: AMAPSim representation of aerial architecture of 50 year old birch (a) and pine (b) tree.

176 **Loading scenarii: allometric laws**

177 The tree is composed of axes organised hierarchically according to their order: 1 for the tree seed, 2 for
 178 the trunk, 3 for the main branches, 4 for those attached to them, and so on. Each axis is described
 179 as a succession of growth units (GU), which are sections of cones, identified by a number (in order of
 180 appearance), and defined by a parent number, an order, a start and end diameter, the coordinates of
 181 the centres of both initial and final sections as well as their length (Fig 3). Note that the description
 182 provided by AmapSim does not include the internal structure of the growth units, such as eccentricity. To
 183 avoid unnecessary complications, the coordinate of the centres will be taken as those of the pith. From the
 184 model data, moments and normal force in each growth unit at any time of the tree's existence can be
 185 computed. Each unit is subjected, in addition to a part of its own weight, to that of its offsprings - this
 186 term referring to any growth unit that would fall if the studied one was cut. The normal force \vec{N}_n and
 187 bending moment \vec{M}_n supported by the growth unit n can be written:

$$\vec{N}_n = \frac{1}{2}m_n\vec{g} + \sum_{\substack{k>n \\ k \text{ of fspring}}} m_k\vec{g} \quad (22)$$

188

$$\vec{M}_n = \overrightarrow{G_n G'_n} \wedge \left(\frac{1}{2}m_n\vec{g} \right) + \sum_{\substack{k>n \\ k \text{ children}}} \overrightarrow{G_n G_k} \wedge (m_k\vec{g}) \quad (23)$$

189 with G_n the centre of gravity of the current growth unit, G'_n that of its second half, on the downstream
 190 side of G_n , G_k that of an offspring of number $k > n$, m_i the mass of growth unit i and \vec{g} the gravity vector.
 191 Once \vec{N}_n and \vec{M}_n are calculated, in the absolute coordinates used for the description of the whole tree,
 192 they are projected in the local coordinate system $(\vec{x}', \vec{y}', \vec{z})$, with \vec{z} of the chosen cross section. In the
 193 following, in accordance with the development of the previous section, N_z will refer to the projection of \vec{N}
 194 on \vec{z} and M_y to that of \vec{M} on \vec{y}' .

195 Power law regressions were performed to recover the allometric coefficients $\lambda_M, \lambda_N, \nu_N, \nu_M$. A summary
 196 of the analysis process is proposed in Figure 3.

197 Branches need to have a long loading history to exhibit interesting stress profiles. Thus, only branches
 198 of order 3 (attached to the trunk) and older than 15 (resp. 17) years were selected in *Pinus pinaster*
 199 (resp. *Prunus avium*). Finally, 64 axes for pine and 65 for cherry wood were identified. The distribution of
 200 all allometric coefficients, for the growth unit closest to the trunk, are presented in Figure 4. In *Pinus*,
 201 there is a large variation in ν -coefficient, with ν_M varying by almost a factor 2 in the studied sample,
 202 indicating very variable secondary growth kinetics. In *Prunus*, the range of variation of the allometric
 203 power coefficients is smaller, which depicts a higher homogeneity of secondary growth kinetics. For both
 204 species, a great diversity in λ -coefficients is observed, which depicts a significant variability in the loading
 205 history. This is particularly interesting as the branches show geometric determinants that do not vary
 206 over large ranges. For example, the radii of the axes considered in *Pinus* vary by only 1.5 cm between
 207 the smallest and largest axis, while the length varies by 20% between the shortest and longest axes. This
 208 reflects the complexity of predicting the loading of a branch from the determinants of the main axis, and
 209 shows the importance of branching. In both cases, these variations in the λ -coefficients result in a factor
 210 of 4 in the bending load between the lightly loaded and the heavily loaded branches.

211 The average values of each allometric and final geometry, indicated in table 1, will be used for the
 212 simulations.

213 **Material data and stem orientation**

214 The stress values in the normal wood were fixed according to the average maturation strains advised by
 215 Thibaut and Gril (2021). Similarly, the green wood MOE were given by the correlation between dry and

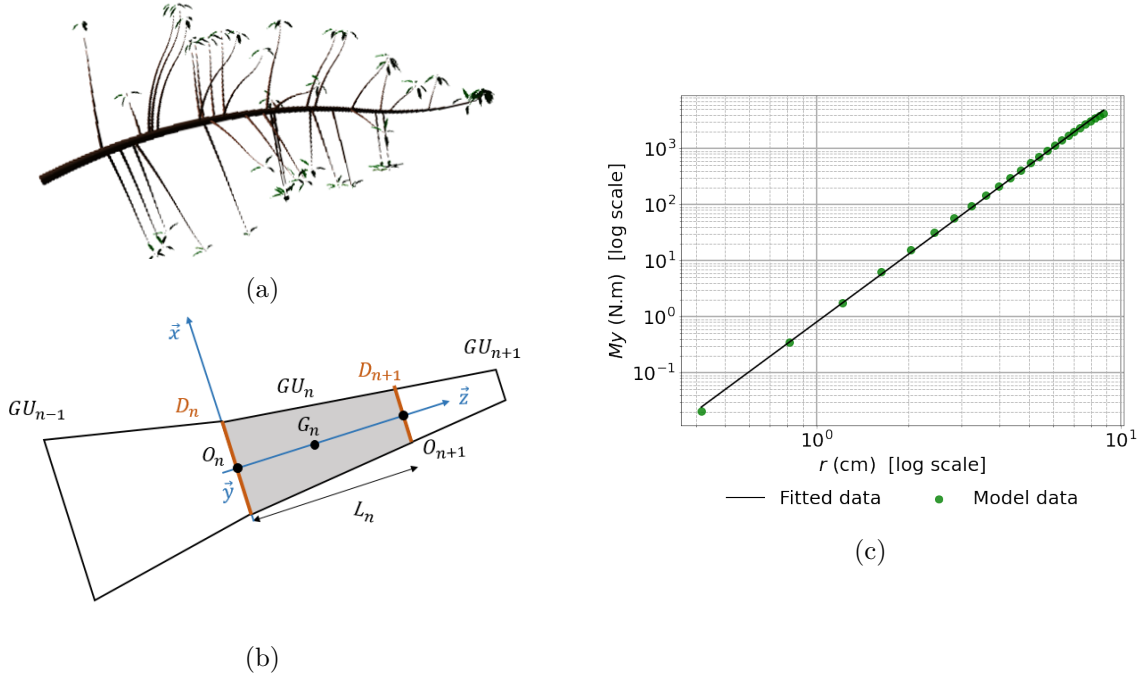


Figure 3: *Prunus avium*. Allometric law. From the geometry of the modeled branche a) and b), the bending moment is calculated. Graph c), The relationship between the branch diameter and the bending moment is plotted. The computation of the fitted curve provides the allometric law.

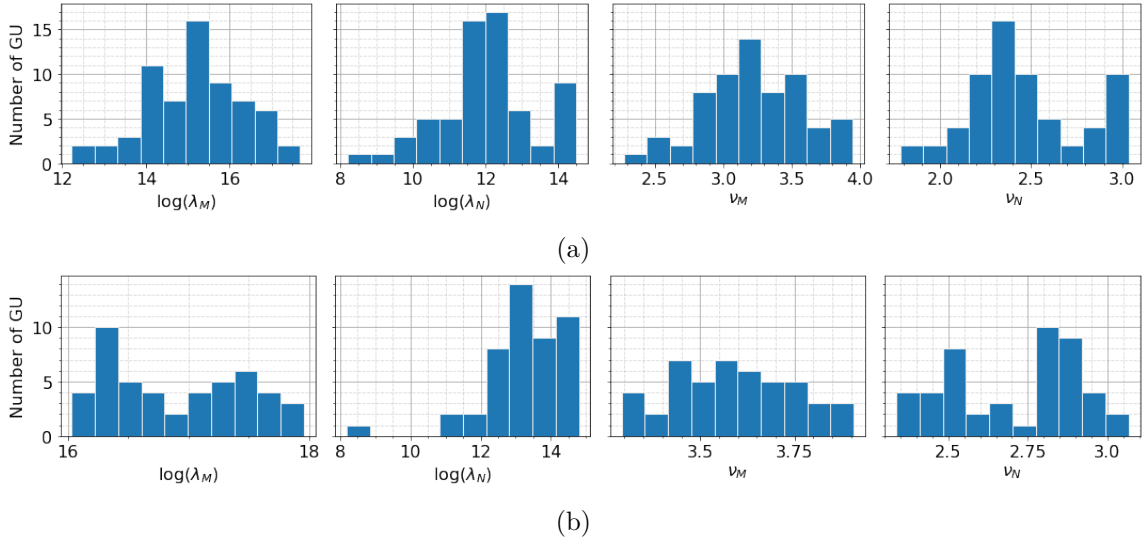


Figure 4: Statistical distribution of allometric coefficients for modelled branches: (a) *Pinus* branches over 15 years old; (b) *Prunus* branches over 17 years old. $\lambda_{M,N}$ refers to the weight, $\nu_{M,N}$ to the kinetic of secondary growth.

216 green MOE identified by Thibaut and Gril (2021): $E_g = 0.89 * E_d$. Dry MOE were provided by the tropix
 217 database of CIRAD [Gérard et al. (2011)]. The density of green wood was approximated by the density of
 218 water $\rho = 1000 \text{ kg.m}^{-3}$. These inputs are summarised in Table 1.
 219 In the following section, the case of stationary growth ($\nu_b = 0$) will be considered principally and analysed
 220 thoroughly. Situations of changing curvature will be then considered briefly.

221

222

Species	$\lambda_M (N.m^{-\nu_M})$	$\lambda_N (N.m^{-\nu_N})$	ν_M	ν_N	$r (cm)$	$\mu_{NW} (\mu\text{strain})$	$E_d (GPa)$	$E_g (GPa)$
<i>Pinus pinae</i>	-6.4e6	5e4	3.2	2.5	5	410	8.8	7.9
<i>Prunus avium</i>	-2.6e7	9.5e3	3.6	2.7	8	712	10.2	9.1

Table 1: Mean input characteristics of the branches

223

Results and discussion

224

Prunus avium: heavily loaded hardwood

225

226

227

228

229

Several postural control scenarii have been computed. First, the ability of the branch to maintain its orientation through RW formation only (Fig 5.a-c) or secondary growth eccentricity only (Fig 5.d-f) is evaluated. Then, combinations of these strategies is proposed (Fig 6): for each combination, one parameter (growth eccentricity or maturation) is assumed to be uniform throughout the growth of the branch, while the other is assumed to be the driver of orientation control.

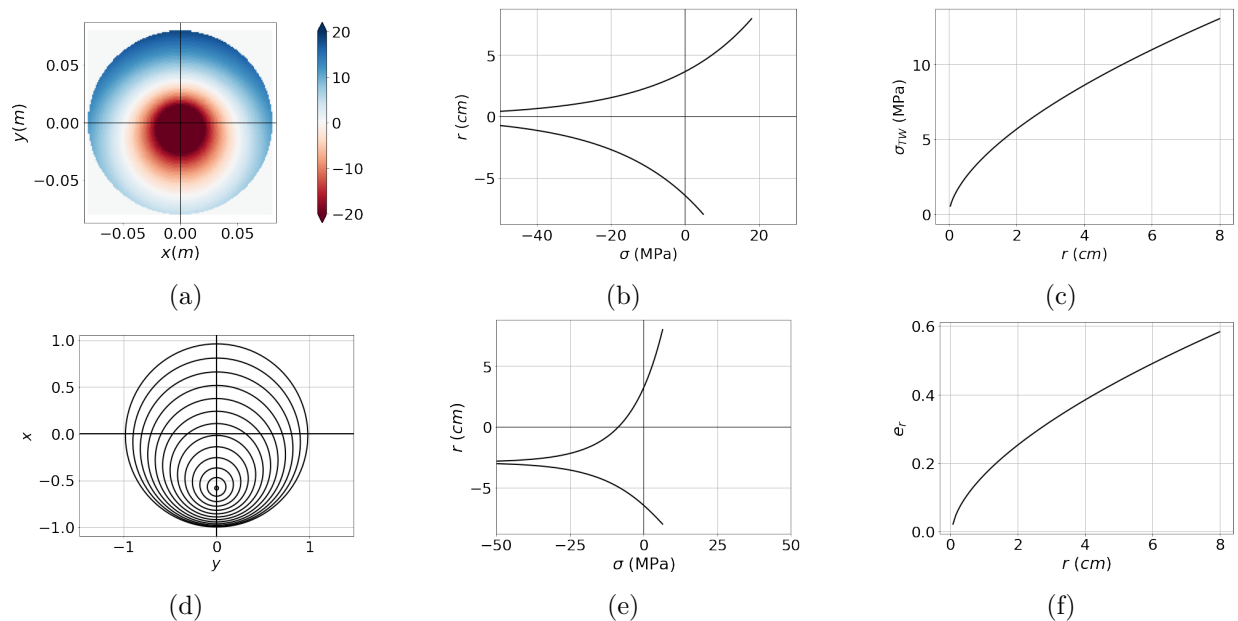


Figure 5: *Prunus avium*: Horizontal orientation maintained by the two different drivers: a-c) maturation stress and d-f) eccentricity. Different types of representation are proposed: a) (resp. d)) 2D visualisation of the growth stress (resp. eccentricity) in the whole section. b) and e) Growth stress profile on the line $y=0$. c) and f) Parametric representation of the tropic driver: maturation stress and eccentricity.

230

231

232

233

234

235

236

237

238

239

Both strategies alone (Fig.5) lead to realistic orders of magnitude (except near the pith, which is an intrinsic limit of our model; this specific point is discussed in section *Limits of the model*). Across the chosen combinations, no single strategy seems to be more efficient than the other. For example, eccentricity alone (5.a-c and 6.b, solid line) may be sufficient to maintain the branch orientation while keeping a sufficient mechanical safety margin ($\max(e) = 0.6$). In comparison, with zero eccentricity (Fig.6.a, dashed line), TW alone leads to a tensile strain $\mu_{RW} \approx 2140\mu\text{strain}$ ($\sigma_{TW} \approx 19.5$ MPa), also far from limits observed in literature [Huang et al. (2005); Thibaut and Gril (2021)]. Moreover, eccentricity and deformation in TW acts as an optimisation of branch control and resistance to breakage: promoting epitrophic eccentricity (more radial growth on the upper side) allows less tension in TW: the more space eccentricity leaves to

240 TW, the lower the stress in it. Interestingly, the worst case (hypotrophic eccentricity, more radial growth
 241 on the lower side, solid line in Fig 6.a) leads to orders of magnitude that are on the border of limits,
 242 but observable: $\mu_{RW} \approx 4970\mu\text{strain}$ ($\sigma_{TW} \approx 45.4 \text{ MPa}$). Note that although for softwoods, there is a
 243 consensus on the eccentricity orientation (hypotrophic) for tropism responses [Timell (1986)], hardwood
 244 species can show eccentricities in both directions [Kucera and Philipson (1977); Wang et al. (2009); Tsai
 245 et al. (2012)]. The hypotrophic eccentricity (Fig 6.a) is obviously not motivated by an optimisation of
 246 postural control, suggesting the existence of trade-offs with other vital functions.
 247 Even if the observation is the same (epitrophic eccentricity lead to less intense TW), graphs 6.b (dashed
 248 and dotted lines) show profiles that have higher safety margins than those in Figure 6.a. When combined,
 249 it seems more efficient to vary the eccentricity and keep a constant difference of maturation stress than
 250 to keep a uniform eccentricity and to vary the maturation stress. To date, there is no study that has
 251 attempted to investigate the variations in space and time of the eccentricity in the branches. This is a
 252 very interesting perspective to understand the interaction between eccentricity, maturation and postural
 253 control of inclined axes.

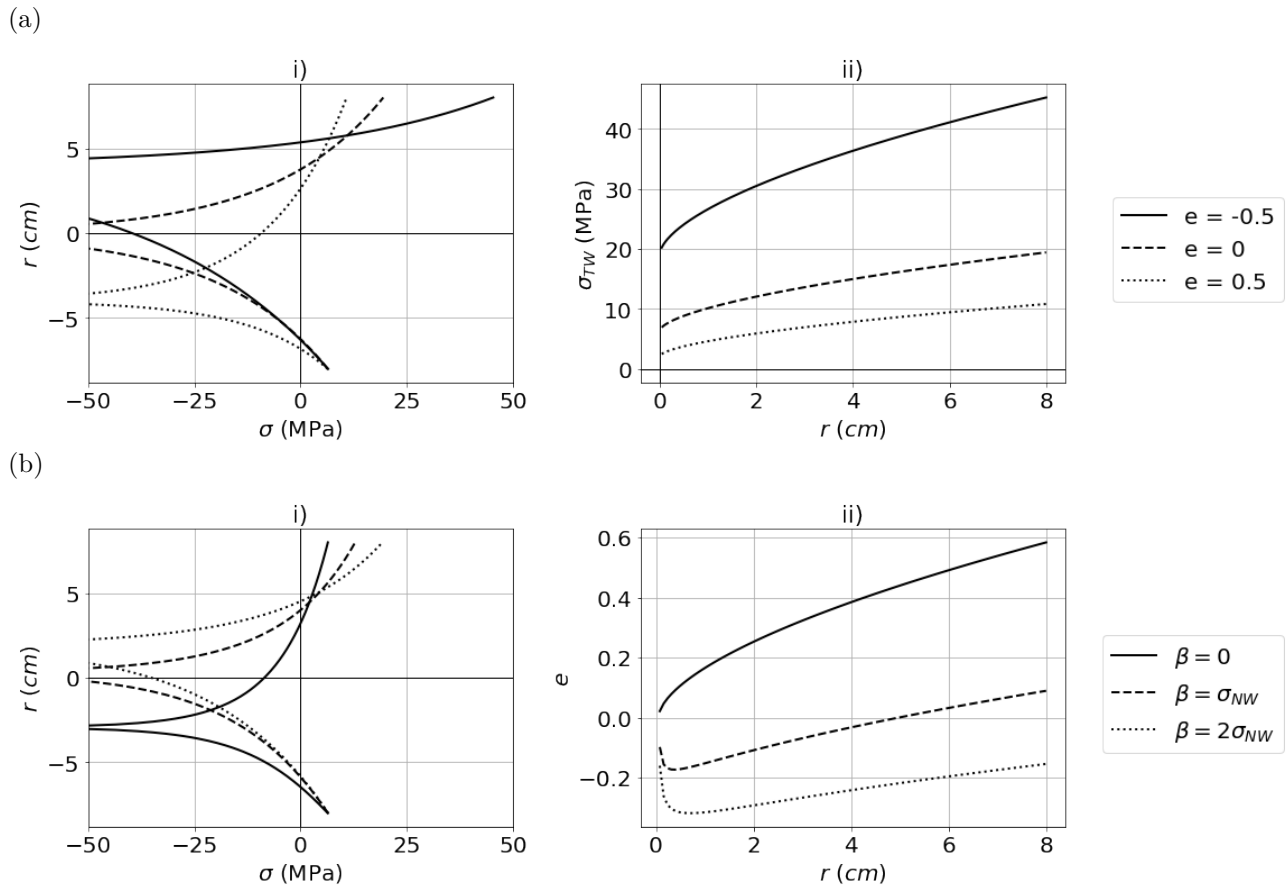


Figure 6: Illustration of different straightening strategies: (a) constant eccentricity, the maturation is the main driver of postural control; (b) constant difference of maturation stress, the eccentricity is the main driver of postural control.

254 ***Pinus pinaster*: lightly loaded softwood**

255 Similarly, for *Pinus pinaster*, we compare the ability of maturation process alone (Fig 7.a-c) and growth
 256 eccentricity alone (Fig 7.d-f) to maintain a constant orientation, then study the combination of these
 257 processes (Figure 8). Note that the average bending moment due to weight is much higher for birch
 258 tree, by a factor roughly 10, than for pine (see λ_M and λ_N in Table 1). This may explain why the

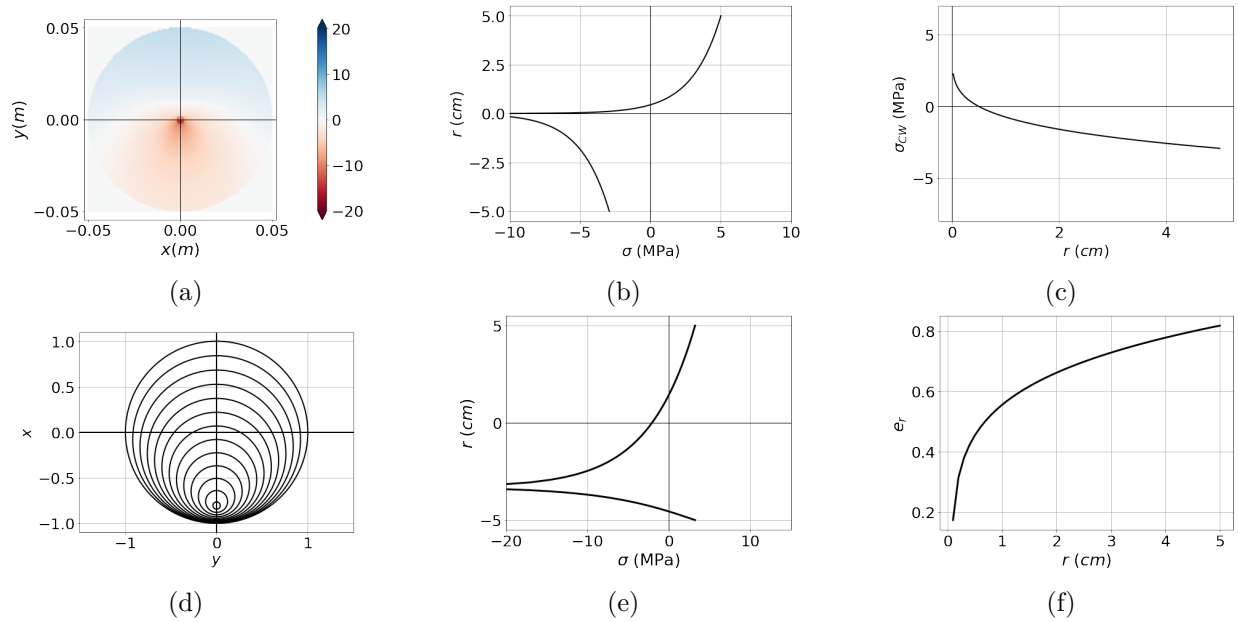


Figure 7: *Pinus pinaster*: Horizontal orientation maintained by the two different drivers: a-c) maturation stress and d-f) eccentricity. Different types of representation are proposed: a) (resp. d)) 2D visualisation of the growth stress (resp. eccentricity) in the whole section. b) and e) Growth stress profile on the line $y=0$. c) and f) Parametric representation of the tropic driver: maturation stress and eccentricity.

259 straightening drivers are much less triggered in the case of this pine. Moreover, in the current model
 260 the Young's modulus is supposed to be uniform in the whole cross section. While this hypothesis does
 261 not have much impact on the stress profiles for hardwoods, where both TW and NW produce tensile
 262 stress and the difference of Young's moduli is moderate, it modifies the results for softwoods much more.
 263 Indeed, although CW of softwoods is typically denser than NW, due to the higher inclination of cellulose
 264 microfibrils, its Young's modulus is often much lower. This explains for a part the commonly observed
 265 association of CW production with eccentric growth. This is an important limitation of the proposed
 266 formulation and will have to be kept in mind when discussing the results.

267 The analysis of each strategy alone (maturation: Fig 7.a-c and Fig.8.a dashed line; eccentricity: Fig 7.d-f
 268 and Fig.8.b solid line) suggests that maturation is more efficient than eccentricity. To ensure the same
 269 growth scenario, the eccentricity alone rises to about 0.8, which is not far from a limit value, whereas
 270 maturation alone leads to low maturation strains in CW ($<500 \mu\text{strain}$, corresponding to 4 MPa). Besides,
 271 this eccentricity is not in the direction of what is commonly observed. This point remains logical, because
 272 without CW, the epitrophic eccentricity leads to shifting the bending centre upward to limit the bending
 273 moment load. Finding an eccentricity opposite to the usual one observed is therefore quite plausible. In
 274 fact, the eccentricity in the early stages of development generates a coordination problem, especially for
 275 softwoods. For hardwoods, the simultaneous building of TW and eccentricity is not an issue, whereas
 276 building a hypotrophic growth pattern without CW is not efficient for softwoods.

277 In case of combined effects, although eccentricity alone ensures stationarity, it does not succeed anymore
 278 when combined to a uniform maturation (red dotted line in Fig. 8.b). For the chosen parameters, this
 279 means that if the maturation strain was higher than $-180 \mu\text{strain}$ ($\sigma_{CW} \approx 1.4 \text{ MPa}$, black dotted line in
 280 Fig. 8.b) the branch could not ensure its orientation using the eccentricity process only. As said before,
 281 the early stages of development in softwood seems to generate coordination problem. Finally, varying the
 282 eccentricity while keeping the maturation stress constant seems to be an irrelevant biomechanical strategy
 283 for the branch. Beyond this result, one can also wonder if this case was realistic: to what extent are there

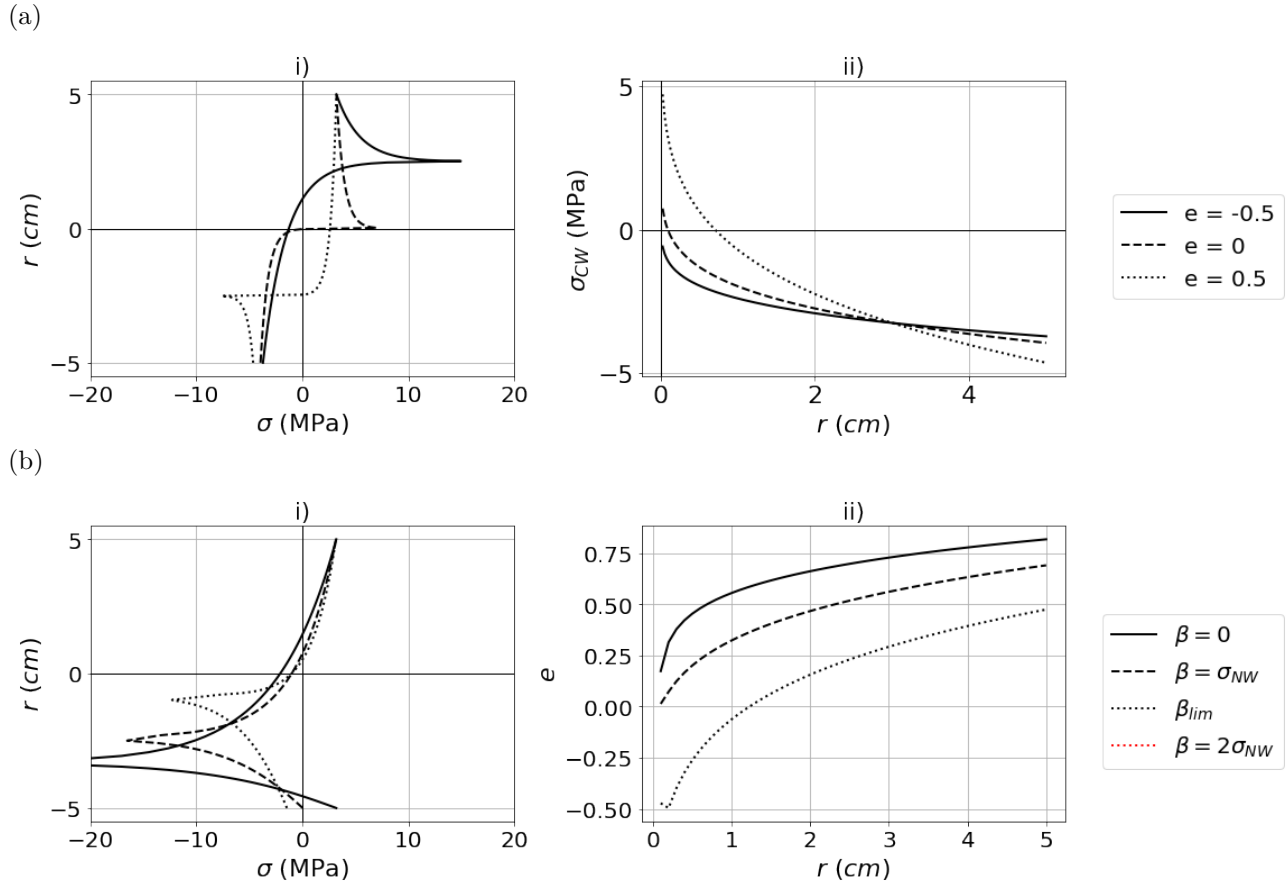


Figure 8: Illustration of different straightening strategies: (a) constant eccentricity, the maturation is the main driver of postural control; (b): constant maturation gradient, the eccentricity is the main driver of postural control.

284 constant maturation constraints throughout the growth of the branches? But if these situations do really
 285 exist, then eccentricity clearly does not have a crucial role in maintaining postural control.

286 For the other combined effects, the eccentricity does not bring much change in the value of the maturation
 287 stress (Fig. 8.a). However, it does not contribute to postural straightening as we initially expected. Indeed,
 288 CW associated with hypotrophic growth shows higher maturation strains than that of epitrophic growth.
 289 This situation occurs when NW has a higher absolute stress than CW. This can be the case for lightly
 290 loaded branches. The hypotrophic eccentricity increases CW effect, but decreases NW effect by the same
 291 amount. If the NW stress is greater in absolute value than in CW, then the branch, in relation to the
 292 straightening requirement, loses more bending moment on the NW side than it gains on the CW side.
 293 In this case, any gradient of hypotrophic eccentricity means geometrical loss of NW action and must be
 294 compensated by an increase in CW stress. Note that "standard" CW has a higher absolute maturation
 295 stress than NW [Thibaut and Gril (2021)]. This situation is illustrated in figure 9. To have a sufficiently
 296 large load, the allometric laws of the heaviest branch of the pine has been used and the final radius
 297 has been set at 8 cm (the same as the average value in the cherry tree). This lead to higher levels of
 298 compression. In this case, the hypotrophy of the eccentricity was well associated with a decrease in CW
 299 intensity. A very interesting question is "why do real branches build CW in cases similar to those we
 300 simulated?" A seductive explanation could be the optimisation of the residual strength of wood: CW is
 301 known to have better compressive strength conferred by its high lignin content and cell wall structure. To
 302 answer this question correctly, it would be necessary to build a fracture model and to include it to our
 303 stress computation model. For example, adding an damage-elastoplastic law would allow to study the

304 effects of stress relaxation and to understand how some profiles that are not optimal for straightening can
 305 possibly be optimal for resisting breakage.

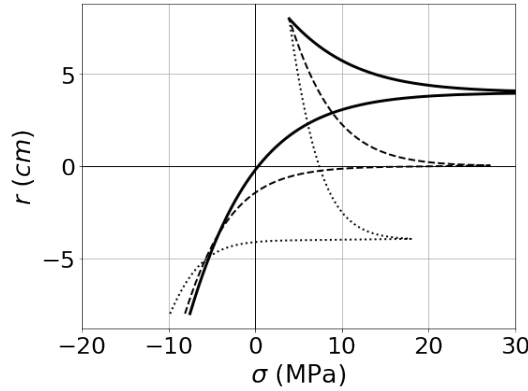
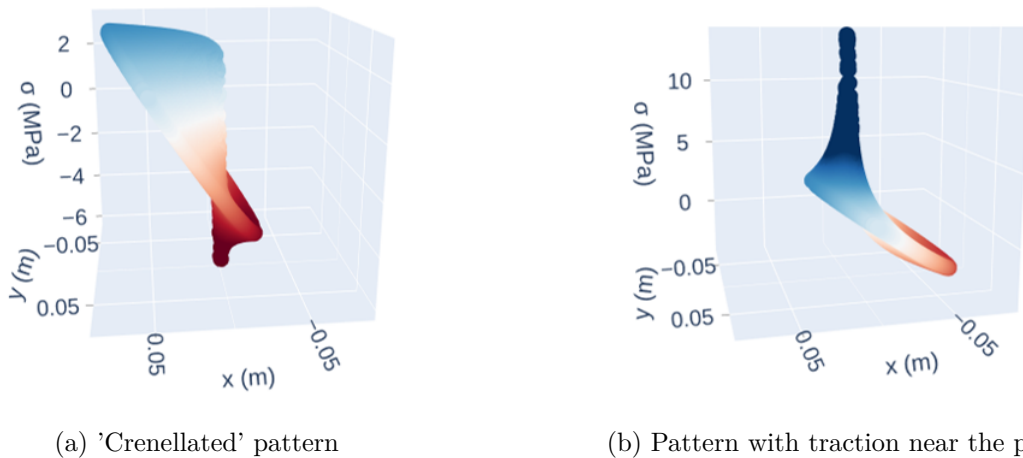


Figure 9: Stress distribution in a the heaviest branch of (*Pinus pinaster*). Different constant eccentricities were imposed (-0.5 for the dotted line, 0 for the dashed and 0.5 for the solid one).

306 Moreover, although the eccentricity process does not play a major role on the evolution of the maturation
 307 stress (Fig.8.a.ii), it considerably modifies the shape of the resulting stress profiles (Fig.8.a.i). Indeed, these
 308 profiles can become 'crenellated' (Fig.8.a.i, dashed curve for zero eccentricity, dotted curve for $e = 0.5$) or
 309 include tension at the pith (solid curve). These two particular patterns are represented in the whole section
 310 in Fig. 10. It seems that before producing tension at the pith, an optimal configuration can be reached for
 311 one specific eccentricity: all the material below the pith 'pushes' the branch and all the material below the
 312 pith 'pulls' it. Ideally, this may be what each branch should tend to do. These results about the branches
 313 mechanical strategies should be compared with experimental measurements.



(a) 'Crenellated' pattern

(b) Pattern with traction near the pith

Figure 10: Spatial distribution of stress in two particular cases in *Pinus pinaster*. a): Case of a uniform epitrophic eccentricity : $e = -0.5$ b). Case of a uniform hypotrophic eccentricity $e = 0.5$. Other input parameters are the same as in Fig 8.

314 Influence of the orientation of the branch: the stationary hypothesis

315 In order to evaluate the relevance of the stationarity hypothesis, different growth scenarios are considered.
 316 For each branch, the case of active straightening or passive bending is modelled. Passive bending is driven
 317 by increasing weight. Up-righting is driven by the maturation gradient, which is set at $400 \mu\text{strain}$ ($\sigma \approx 3.2$
 318 MPa)for pine and $700 \mu\text{strain}$ ($\sigma \approx 6.2$ MPa) for birch tree (the gradient is of the order of magnitude

319 of NW stress). The results are shown in Figure 11. In birch, no major change of the stress pattern is
 320 observed. In contrast, the pattern changes greatly for pine. For a passive-bending branch, a 'V' profile
 321 and the absence of CW are observed. For straightening, the previously-mentioned profile with tension
 322 at the pith is observed. In both cases, the orders of magnitude are compatible with a mechanical safety
 323 margin for the branches. Apart from modified tropisms (change of light environment, weight change by
 324 loss of part of the branch, etc.), the maintaining of the orientation is quite common for real branches. The
 325 simulations suggest, however, that if for any reason they need to modify their orientation, they can do it
 326 without taking too much mechanical risk. The hypothesis of branch direction stationarity is totally in
 327 accordance with the long term mechanical requirements needed during the building of branches.

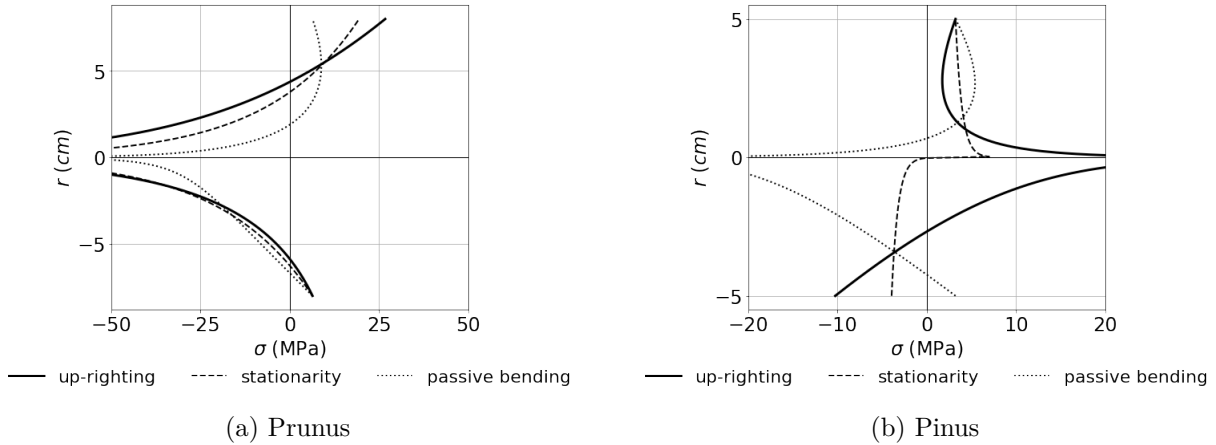


Figure 11: Distribution of growth stresses for different orientation scenarios.

328 **About the hypothesis of the preponderance of the vertical bending moment over the horizontal**
 329 **bending and torsion moments**

330 One of the initial hypothesis of our model was that the vertical bending moment (M_y in our formalism)
 331 prevails over the torsional moment M_z and horizontal bending moment M_x . This allowed to consider only
 332 one direction of eccentricity and to avoid all the non-linear terms generated by the torsional components.
 333 We evaluated the maximum values of the three moments for all modeled branches of each species for
 334 comparison purpose. The results are presented in figure 12. They enlighten that for every comparison,
 335 the vertical moment shows much higher values than the torsional and horizontal bending moments and
 336 validates our initial hypothesis.

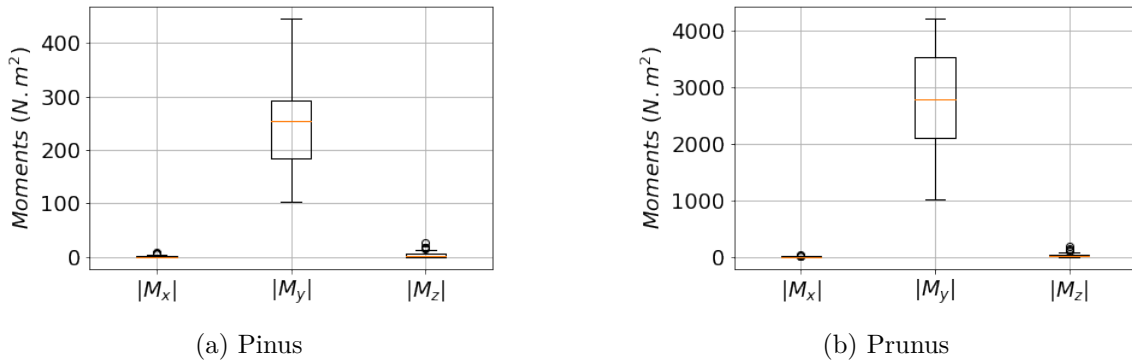


Figure 12: Comparison of maximum moments for modeled branches. M_x : horizontal moment; M_y : vertical moment; M_z : torsional moment.

337 Limits of the model

338 The evaluation of the stress during the first stages of stem development is an issue of the model. In almost
339 every stress profiles, at the pith a tension or compression peak is obtained, generally exceeding wood
340 strength, which is not compatible with branch sustainability. This point could be corrected in two ways.
341 First, the role of the bark could be taken into account. Its mechanical role for small axes has already
342 been studied and its importance in postural straightening was clearly highlighted [Clair et al. (2019);
343 Ghislain et al. (2019)]. Our model could include the mechanical action of bark in the early stages of
344 branch development. This improvement would require additional data about the mechanical behaviour of
345 the bark but would bring more realistic stress predictions and limit the artefacts at the pith. A second
346 exciting perspective would be to take into account the elastoplastic behaviour of wood. By imposing a
347 realistic plastic strain limit, the peak at the pith would then disappear; and the increments would be
348 spread over the middle part of the section, thus modifying the odd pattern observed in figure 10.

349 A another limit is the hypothesis about wood stiffness. It is particularly unfavourable for softwoods,
350 because it reinforces some geometric phenomena (see the one in Fig.8.a.i). In this context, it would be
351 very interesting to evaluate the potential link between eccentricity and modulus variations. If the latter is
352 established, the eccentricity that we would impose with the model would serve to compensate or amplify
353 the effect of the tension wood. However, it remains unclear whether or not this would explain the limited
354 action available to the branch in the case of a constant maturation stress.

355 Conclusion and perspectives

356 A semi-analytical growth stress model has been developed a in the context of branch development. At each
357 radius increment, the stress balance is computed in order to fit with a given curvature. A first novelty of
358 this model is that it takes into account the role of the eccentricity variation in time. A second contribution
359 is that it computes the stress distribution in the whole cross-section. It has been applied to test the
360 effectiveness of two well-known biomechanical strategies of woody plants to control the orientation of their
361 stem: secondary growth eccentricity and reaction wood formation. The case of softwood and hardwood
362 branches were computed using digital data provided by AMAPSim software. For hardwood, growth stress
363 simulations show that both strategies are efficient to maintain a given orientation, although eccentricity is
364 more so than the generation of maturation gradients. On the contrary, in the case of softwood, reaction
365 wood formation appears to be more efficient than eccentric growth. Obviously, in all cases, the combination
366 of both processes yields very high stress levels that are able to keep the branch straight or modify its
367 orientation. Few strategies, such as forming reaction wood uniformly over time while allowing eccentric
368 growth, are not optimal to maintain the orientation. However, since growth eccentricity does not play a
369 major role in straightening capabilities, it does not influence much the shape of the stress profiles. Few odd
370 and critical profiles "in crenelated" or "with traction" near the pith have been identified. Their analysis
371 provides very exciting perspectives for further experimental works in order to get real data. Finally, for
372 lightly loaded softwood branches, the eccentric growth plays a minor role in straightening. The model is
373 limited in terms of predicting capacity because of the lack of experimental data.

374 Now that a complete model is available, it becomes crucial to start experimental investigations in order
375 to compare the outputs with real in situ observations. Especially, we need to evaluate the relevance of
376 the different scenarii (constant gradient, constant eccentricity). The question of the relevance of the
377 stationarity of the branch's trajectory hypothesis has been also established. In particular, we have shown
378 that the branch could deviate from a stationary trajectory without limiting its mechanical strength too
379 much.

380 A key point for understanding branch sizing is the question of biomass costs. Building additional wood
381 on one side or forming reaction wood are carbon sinks with possible trade-offs. One perspective of work
382 would be to affect a cost to the production of reaction wood as well as to eccentric growth. The resulting

383 computations could then help to understand the choice of some strategies over others and would lead to
384 coupling the biomechanical point of view to other biological considerations.

385 References

- 386 T. Alméras, D. Jullien, and J. Gril. *Modelling, Evaluation and Biomechanical Consequences of Growth Stress*
387 *Profiles Inside Tree Stems*, pages 21–48. Springer International Publishing, Cham, 2018. ISBN 978-3-319-
388 79099-2. doi: 10.1007/978-3-319-79099-2_2. URL https://doi.org/10.1007/978-3-319-79099-2_2.
- 389 T. Alméras and B. Clair. Critical review on the mechanisms of maturation stress generation in trees.
390 *Journal of The Royal Society Interface*, 13(122):20160550, 2016. doi: 10.1098/rsif.2016.0550. URL
391 <https://royalsocietypublishing.org/doi/abs/10.1098/rsif.2016.0550>.
- 392 T. Alméras and M. Fournier. Biomechanical design and long-term stability of trees: Morphological and
393 wood traits involved in the balance between weight increase and the gravitropic reaction. *Journal of*
394 *Theoretical Biology*, 256(3):370–381, 2009. ISSN 0022-5193. URL [http://www.sciencedirect.com/
395 science/article/pii/S0022519308005389](http://www.sciencedirect.com/science/article/pii/S0022519308005389).
- 396 T. Alméras, A. Thibaut, and J. Gril. Effect of circumferential heterogeneity of wood maturation strain,
397 modulus of elasticity and radial growth on the regulation of stem orientation in trees. *Trees*, 19(4):
398 457–467, 2005. ISSN 1432-2285. URL <https://doi.org/10.1007/s00468-005-0407-6>.
- 399 P. Ancelin, T. Fourcaud, and P. Lac. Modelling the biomechanical behaviour of growing trees at the forest
400 stand scale. part i: Development of an incremental transfer matrix method and application to simplified
401 tree structures. *Annals of Forest Science*, 61(3):263–275, 2004.
- 402 R. R. Archer. On the distribution of tree growth stresses. ii. stresses due to asymmetric growth strains.
403 *Wood Science and Technology*, V10:293–309, 1976.
- 404 R. R. Archer and F. E. Byrnes. On the distribution of tree growth stresses – part i: An anisotropic
405 plane strain theory. *Wood Science and Technology*, 8(3):184–196, 1974. ISSN 1432-5225. URL
406 <https://doi.org/10.1007/BF00352022>.
- 407 J.-F. Barczi, H. Rey, Y. Caraglio, P. de Reffye, D. Barthélémy, Q. X. Dong, and T. Fourcaud. AmapSim:
408 A Structural Whole-plant Simulator Based on Botanical Knowledge and Designed to Host External
409 Functional Models. *Annals of Botany*, 101(8):1125–1138, 09 2007. ISSN 0305-7364. doi: 10.1093/aob/
410 mcm194. URL <https://doi.org/10.1093/aob/mcm194>.
- 411 D. Barthélémy, Y. Caraglio, and S. Sabatier. 4.1 crown architecture of valuable broadleaved species.
412 *Valuable broadleaved forests in Europe*, 22:87, 2009.
- 413 D. Barthélémy and Y. Caraglio. Plant Architecture: A Dynamic, Multilevel and Comprehensive Approach
414 to Plant Form, Structure and Ontogeny. *Annals of Botany*, 99(3):375–407, 01 2007. ISSN 0305-7364.
415 doi: 10.1093/aob/mcl260. URL <https://doi.org/10.1093/aob/mcl260>.
- 416 Y. Caraglio. Le développement architectural du merisier. *Forêt Entreprise 107*, (107):72–80, 1996.
- 417 B. Clair, B. Ghislain, J. Prunier, R. Lehnebach, J. Beauchêne, and T. Alméras. Mechanical contribution
418 of secondary phloem to postural control in trees: the bark side of the force. *New Phytologist*, 221(1):
419 209–217, 2019. doi: <https://doi.org/10.1111/nph.15375>. URL [https://nph.onlinelibrary.wiley.
420 com/doi/abs/10.1111/nph.15375](https://nph.onlinelibrary.wiley.com/doi/abs/10.1111/nph.15375).
- 421 T. Coudurier, D. Barthelemy, B. Chanson, F. Courdier, and C. Loup. Premier résultats sur la modélisation
422 du pin maritime pinus pinaster ait.(pinecae). *Architecture des arbres fruitiers et forestiers*, page 306,
423 1993.

- 424 C. Coutand, M. Fournier, and B. Moulia. The gravitropic response of poplar trunks: Key roles of
425 prestressed wood regulation and the relative kinetics of cambial growth versus wood maturation.
426 *Plant Physiology*, 144(2):1166–1180, 2007. ISSN 0032-0889. doi: 10.1104/pp.106.088153. URL <http://www.plantphysiol.org/content/144/2/1166>.
427
- 428 J. B. Fisher and J. W. Stevenson. Occurrence of reaction wood in branches of dicotyledons and its
429 role in tree architecture. *Botanical Gazette*, 142(1):82–95, 1981. doi: 10.1086/337199. URL <https://doi.org/10.1086/337199>.
430
- 431 T. Fourcaud, F. Blaise, P. Lac, P. Castéra, and P. de Reffye. Numerical modelling of shape regulation and
432 growth stresses in trees. *Trees*, 17(1):31–39, 2003. ISSN 1432-2285. URL <https://doi.org/10.1007/s00468-002-0203-5>.
433
- 434 M. Fournier, B. Chanson, D. Guitard, and B. Thibault. Mécanique de l’arbre sur pied : modélisation d’une
435 structure en croissance soumise à des chargements permanents et évolutifs. 1. analyse des contraintes de
436 support. 1991a.
- 437 M. Fournier, B. Chanson, D. Guitard, and B. Thibault. Mécanique de l’arbre sur pied : modélisation d’une
438 structure en croissance soumise à des chargements permanents et évolutifs. 2. analyse tridimensionnelle
439 des contraintes de maturation, cas du feuillu standard. 1991b.
- 440 M. Fournier, H. Baillères, and B. Chanson. Tree biomechanics : growth, cumulative prestresses, and
441 reorientations. *Biomimetics*, 2(3):229–251, 1994.
- 442 B. Ghislain, T. Alméras, J. Prunier, and B. Clair. Contributions of bark and tension wood and role of the
443 g-layer lignification in the gravitropic movements of 21 tropical tree species. *Annals of Forest Science*,
444 76(4):107, 2019. ISSN 1297-966X. URL <https://doi.org/10.1007/s13595-019-0899-7>.
- 445 J. Gérard, D. Guibal, S. Paradis, M. Vernay, J. Beauchêne, L. Brancheriau, I. Châlon, C. Daigremont,
446 P. Détienne, D. Fouquet, P. Langbour, S. Lotte, M.-F. Thévenon, C. Méjean, and A. Thibaut. Tropix 7,
447 2011. URL <http://tropix.cirad.fr/en>.
- 448 F. Hallé, R. A. Oldeman, and P. B. Tomlinson. *Tropical trees and forests: an architectural analysis*.
449 Springer Verlag, 1978.
- 450 P. Heuret, C. Meredieu, T. Coudurier, F. Courdier, and D. Barthélémy. Ontogenetic trends in the
451 morphological features of main stem annual shoots of pinus pinaster (pinaceae). *American Journal of*
452 *Botany*, 93(11):1577–1587, 2006. doi: <https://doi.org/10.3732/ajb.93.11.1577>. URL <https://bsapubs.onlinelibrary.wiley.com/doi/abs/10.3732/ajb.93.11.1577>.
453
- 454 Y.-S. Huang, S.-S. Chen, L.-L. Kuo-Huang, and C.-M. Lee. Growth strain in the trunk and branches of
455 chamaecyparis formosensis and its influence on tree form. *Tree Physiol*, 25(9):1119–1126, Sept. 2005.
456 ISSN 0829-318X. URL <https://doi.org/10.1093/treephys/25.9.1119>.
- 457 Y.-S. Huang, L.-F. Hung, and L.-L. Kuo-Huang. Biomechanical modeling of gravitropic response of
458 branches: roles of asymmetric periphery growth strain versus self-weight bending effect. *Trees*, 24(6):
459 1151–1161, 2010. ISSN 1432-2285. URL <https://doi.org/10.1007/s00468-010-0491-0>.
- 460 L.-F. Hung, C.-C. Tsai, S.-J. Chen, Y.-S. Huang, and L.-L. Kuo-Huang. Study of tension wood in
461 the artificially inclined seedlings of koelreuteria henryi dummer and its biomechanical function of
462 negative gravitropism. *Trees*, 30(3):609–625, 2016. ISSN 1432-2285. URL <https://doi.org/10.1007/s00468-015-1304-2>.
463
- 464 L.-F. Hung, C.-C. Tsai, S.-J. Chen, Y.-S. Huang, and L.-L. Kuo-Huang. Strain distribution, growth
465 eccentricity, and tension wood distribution in the plagiotropic and orthotropic branches of koelreuteria

- 466 henryi dummer. *Trees*, 31(1):149–164, 2017. ISSN 1432-2285. URL <https://doi.org/10.1007/s00468-016-1464-8>.
467
- 468 L. J. Kucera and W. R. Philipson. Growth eccentricity and reaction anatomy in branchwood of drimys
469 winteri and five native new zealand trees. *New Zealand Journal of Botany*, 15(3):517–524, 1977. doi:
470 10.1080/0028825X.1977.10429625. URL <https://doi.org/10.1080/0028825X.1977.10429625>.
- 471 H. Kübler. Studien über wachstumsspannungen des holzes iii. längenänderungen bei der wärmebehandlung
472 frischen holzes. *Holz Rohst Werkst*, 17(3):77–86, 1959.
- 473 J. E. Nicholson. A rapid method for estimating longitudinal growth stresses in logs. *Wood Science and
474 Technology*, 5(1):40–48, 1971. ISSN 1432-5225. URL <https://doi.org/10.1007/BF00363119>.
- 475 B. Thibaut. Three-dimensional printing, muscles, and skeleton: mechanical functions of living wood.
476 *Journal of Experimental Botany*, 70(14):3453–3466, 04 2019. ISSN 0022-0957. doi: 10.1093/jxb/erz153.
477 URL <https://doi.org/10.1093/jxb/erz153>.
- 478 B. Thibaut and J. Gril. Tree growth forces and wood properties. *Peer Community Journal*, 1:e46, 2021. doi:
479 10.24072/pcjournal.48. URL [https://peercommunityjournal.org/articles/10.24072/pcjournal.
480 48/](https://peercommunityjournal.org/articles/10.24072/pcjournal.48/).
- 481 T. E. Timell. *Compression wood in gymnosperms*, volume 1. Springer, 1986.
- 482 C.-C. Tsai, L.-F. Hung, C.-T. Chien, S.-J. Chen, Y.-S. Huang, and L.-L. Kuo-Huang. Biomechanical
483 features of eccentric cambial growth and reaction wood formation in broadleaf tree branches. *Trees*, 26
484 (5):1585–1595, 2012. ISSN 1432-2285. URL <https://doi.org/10.1007/s00468-012-0733-4>.
- 485 Y. Wang, J. Gril, and J. Sugiyama. Is the branch of viburnum odoratissimum var. awabuki reaction
486 wood? unusual eccentric growth and various distributions of growth strain. In *6th Plant Biomechanics
487 Conference*, pages 328–334, 2009.
- 488 H. Yamamoto, M. Yoshida, and T. Okuyama. Growth stress controls negative gravitropism in woody
489 plant stems. *Planta*, 216(2):280–292, 2002. ISSN 1432-2048. URL [https://doi.org/10.1007/
490 s00425-002-0846-x](https://doi.org/10.1007/s00425-002-0846-x).
- 491 J. L. Yang, H. Baillères, T. Okuyama, A. Muneri, and G. Downes. Measurement methods for longitudinal
492 surface strain in trees: a review. *Australian Forestry*, 68(1):34–43, 2005. doi: 10.1080/00049158.2005.
493 10676224. URL <https://doi.org/10.1080/00049158.2005.10676224>.
- 494 M. Yoshida and T. Okuyama. Techniques for measuring growth stress on the xylem surface using strain
495 and dial gauges. 56(5):461–467, 2002. doi: doi:10.1515/HF.2002.071. URL [https://doi.org/10.1515/
496 HF.2002.071](https://doi.org/10.1515/HF.2002.071).

497 **Appendix A**

498 The calculation of integrals of the system 3 needs some preliminary elements. The situation of two
 499 consecutive rings is represented in figure 13. Each position x in the geometrical reference frame is expressed
 500 with respect to the position x' in the pith reference frame according to the equation:

$$x = r \cos \theta = x' - \bar{e}R \quad (24)$$

with r the radius at time t and R the radius at the final time.

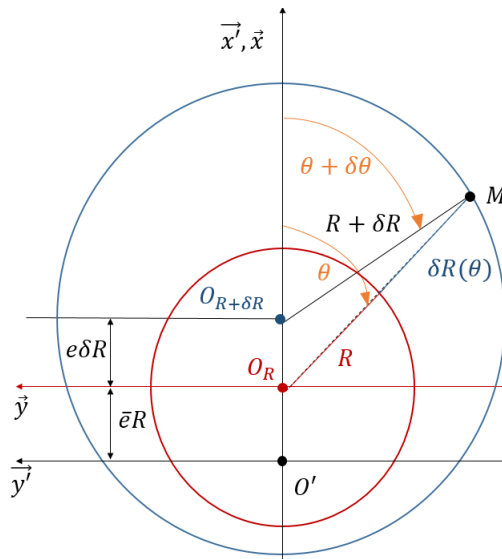


Figure 13: Representation of two consecutive rings and the elements needed to calculate $\delta R(\theta)$

501

502 Then, the integrals of the system 3 are computed as follows:

$$\begin{aligned} \int_s \delta \sigma ds &= \int_s E [\delta a + (x + \bar{e}.R)\delta b] r \delta r d\theta \\ &= E\pi R^2 (\delta a + \bar{e}.R\delta b) \\ \int_s x' \delta \sigma ds &= \int_s [\delta a + (x + \bar{e}.R)\delta b] [x + \bar{e}.R] r \delta r d\theta \\ &= E\pi R^3 \left[\bar{e}\delta a + R \left(\bar{e}^2 + \frac{1}{4} \right) \delta b \right] \end{aligned}$$

The tangential distribution of the radius increment $\delta R(\theta)$ are required in order to compute the terms of maturation. The Figure 13, enlighten that $\overrightarrow{OM} + \overrightarrow{MO'} = \overrightarrow{OO'}$:

$$\begin{cases} [R + \delta R(\theta)] \cos \theta - (R + \delta R) \cos (\theta + \delta \theta) = e_R \delta R & (25a) \\ [R + \delta R(\theta)] \sin \theta - (R + \delta R) \sin (\theta + \delta \theta) = 0 & (25b) \end{cases}$$

503 By setting $\delta \theta \rightarrow 0$, it comes:

$$\begin{cases} \cos (\theta + \delta \theta) = \cos \theta - \sin \theta \delta \theta & (26a) \\ \sin (\theta + \delta \theta) = \sin \theta + \cos \theta \delta \theta & (26b) \end{cases}$$

504 Substituting 26 into 25, and using the combination 25a.cos θ + 25b.sin θ , $\delta R(\theta)$ can finally be written as:

$$\boxed{\delta R(\theta) = \delta R [1 + e_R \cos \theta]} \quad (27)$$

Then:

$$\begin{aligned} \int_{\delta s} \sigma_0^i ds &= \int_{\delta s} \sigma_0^i(\theta) R \delta R(\theta) d\theta \\ &= \int_{\delta s} [\alpha + \beta \cos \theta] [1 + e \cos \theta] R \delta R(\theta) d\theta \\ &= \pi (2\alpha + e\beta) R \delta R \\ \int_{\delta s} x' \sigma_0^i ds &= \int_{\delta s} \sigma_0^i(\theta) (x + e.R) R \delta R(\theta) d\theta \\ &= R^2 \delta R \pi (3\alpha e + \beta e^2 + \beta) \end{aligned}$$

505 Appendix B

The matrix system 7 becomes:

$$\begin{cases} \delta a = \frac{\delta F_0 K_2 - \delta F_1 K_1}{K_0 K_2 - K_1^2} & (28a) \\ \delta b = \frac{\delta F_0 K_1 - \delta F_1 K_0}{K_1^2 - K_0 K_2} & (28b) \end{cases}$$

506 Then, numerators and denominators are calculated separately:

$$K_0 K_2 - K_1^2 = E^2 \pi^2 R^6 \left(\bar{e}^2 + \frac{1}{4} \right) - E^2 \pi^2 R^6 \bar{e}^2 = \frac{(E\pi R^3)^2}{4}$$

$$\begin{aligned} \delta F_0 K_2 - \delta F_1 K_1 &= E\pi^2 R^5 \left[-(2\alpha + e\beta) \left(\bar{e}^2 + \frac{1}{4} \right) + \bar{e} (3\alpha e + \beta e^2 + \beta) \right] \delta R + E\pi R^3 \left[R\delta N \left(\bar{e}^2 + \frac{1}{4} \right) - \bar{e}\delta M \right] \\ &= E\pi^2 R^5 \left[\alpha \left(3e\bar{e} - 2\bar{e}^2 - \frac{1}{2} \right) + \beta \left(\bar{e} - \frac{e}{4} \right) \right] \delta R + E\pi R^3 \left[R\delta N \left(\bar{e}^2 + \frac{1}{4} \right) - \bar{e}\delta M \right] \end{aligned}$$

$$\begin{aligned} \delta F_0 K_1 - \delta F_1 K_0 &= E\pi^2 R^4 \left[-\bar{e} (2\alpha + e\beta) + (3\alpha e + e^2\beta + \beta) \right] \delta R + E\pi R^2 [\bar{e}R\delta N - \delta M] \\ &= E\pi^2 R^4 \left[\alpha (3e - 2\bar{e}) + \beta (1 + e^2 - e\bar{e}) \right] \delta R + E\pi R^2 [\bar{e}R\delta N - \delta M] \end{aligned}$$

Putting the calculations together, system 28 becomes:

$$\begin{cases} \delta a = \frac{4}{ER} \left[\alpha \left(3e\bar{e} - 2\bar{e}^2 - \frac{1}{2} \right) + \beta \left(\bar{e} - \frac{e}{4} \right) \right] \delta R + \frac{4}{E\pi R^3} \left[R\delta N \left(\bar{e}^2 + \frac{1}{4} \right) - \bar{e}\delta M \right] \\ \delta b = \frac{4}{ER^2} \left[\alpha (3e - 2\bar{e}) + \beta (1 + e^2 - e\bar{e}) \right] \delta R + \frac{4}{E\pi R^4} [\bar{e}R\delta N - \delta M] \end{cases}$$

507 Appendix C

508 The following calculus is based on Figure 3.b). To get the vertical bending moment M_y of unit n (eq 23),
 509 one need the calculation of each volume V_n and center of gravity G_n . Lets fix $D(z)$ the deflection of the
 510 cone. It comes:

$$V_n = \int_0^{L_n} \frac{\pi D(z)^2}{4} dz \quad (30)$$

511 where $D(z) = D_n + \left(\frac{D_{n+1}-D_n}{L_n}\right)z$. One gives

$$O_n G_n = \frac{1}{V_n} \int_0^{L_n} \frac{\pi D(z)^2}{4} z dz \quad (31)$$

Setting $\gamma = \frac{D_{n+1}-D_n}{D_n}$ and $\xi = \frac{L_n}{z}$, the equation 30 and 31 then become:

$$V_n = \frac{\pi D_n^2 L_n}{4} \int_0^1 (1 + \gamma \xi)^2 d\xi = \frac{\pi D_n^2 L_n}{4} \cdot \left(1 + \gamma + \frac{\gamma^2}{3}\right)$$

$$O_n G_n = \frac{1}{V_n} \frac{\pi D_n^2 L_n^2}{4} \cdot \left(\frac{1}{2} + \frac{2\gamma}{3} + \frac{\gamma^2}{4}\right)$$

512 So, finally, $O_n G_n$ can be written:

$$O_n G_n = \frac{L_n}{2} \left(\frac{1 + \frac{4}{3}\gamma + \frac{1}{2}\gamma^2}{1 + \gamma + \frac{1}{3}\gamma^2} \right) \quad (32)$$